Mechanism and Machine Theory 46 (2011) 1840–1853

Contents lists available at ScienceDirect

Mechanism and Machine Theory

journal homepage: www.elsevier.com/locate/mechmt

# Mathematical model and tooth surfaces of recess action worm gears with double-depth teeth

Wei-Liang Chen [a], Chung-Biau Tsay [b,*]

[a] Department of Mechanical Engineering, National Chiao Tung University, Hsinchu 30010, Taiwan
[b] Department of Mechanical and Computer-Aided Engineering, Feng Chia University, Taichung 40724, Taiwan

ARTICLE INFO

*Article history:*
Received 28 September 2010
Received in revised form 9 July 2011
Accepted 21 July 2011

*Keywords:*
Recess action
Double-depth teeth
RA worm gear
Tooth surface variation

ABSTRACT

In this study, the surface equations of recess action (RA) worm gears with double-depth teeth, generated by a ZN worm-type hob cutter, are proposed. Based on the generation mechanism and the theory of gearing, a mathematical model of a series of worm gears, semi RA, full RA and standard proportional tooth types, with double-depth teeth is developed as the function of design parameters of the ZN worm-type hob cutter. According to the derived tooth surface equations, computer graphs of a series of worm gears with double-depth teeth are plotted. Tooth surface variations of the generated RA worm gears due to the varying pitch line, pressure angle and tooth height of the hob cutter are also investigated.



## 1. Introduction

Majority of gears are used to transfer power or torque. Few of gears, such as indexing gears, are applied to transmit precise control of angular motion, and transferring of power or torque becomes their secondary consideration. Some of indexing gears usually operate in the open air, or only use grease lubrication, especially that are used to drive military weapons, radio telescopes, satellite tracking antennas, etc. They need to run under the conditions of lower friction, more smooth and stable than equivalent gears. It is well-known that recess action gears (abbreviated to RA gears) have less wear with lower friction and less noise [1].

Buckingham [1] interpreted that friction of recess action is lower than that of approach action when gears are in meshing. Buckingham [2] also indicated that one of worm gear drives, the deep-tooth cylindrical worm drive, was manufactured by Delava-Holroyd Inc. and employed to precise rotation of the heavy 200-in. Mt. Palomar telescope. It has also been applied to a large range of finders. This worm gear drive is similar to that of the convectional type, but it is actually modified into a full RA worm gear drive with double-depth teeth and low pressure angle. Compared with the conventional type of worm gear drive, these modifications result in a large number of teeth in contact and high recess action inducing lower friction. Benefit of multiple tooth contact not only reduces kinematic errors but also averages the sum of all tooth errors. Crosher [3] interpreted that Zahnradfabrik OTT in Germany has developed worm gear sets having a small backlash, and OTT's specifications were also satisfied minimum total composite error in precise positioning. They were designed with a very high contact ratio (CR) in order to have a uniform and constant contact. This can be achieved with a low pressure angle, very long tooth flanks and a large number of worm gear teeth, etc. However, the limitation is the narrowness at the top of the teeth and the worm helix. Shigley and Mischke [4] defined CR of a gear pair as the average number of teeth in contact during the gear meshing. Therefore, the CR of an RA worm gear drive can be calculated by the rotational angle of a gear tooth, measured from the beginning contact point to the end contact point which can be calculated by applying the tooth contact analysis (TCA) results, divided by the angle formed by two successive teeth.

* Corresponding author.
*E-mail address:* cbtsay@mail.nctu.edu.tw (C.-B. Tsay).

0094-114X/$ – see front matter © 2011 Elsevier Ltd. All rights reserved.
doi:10.1016/j.mechmachtheory.2011.07.015

**Nomenclatures**

| | |
|---|---|
| $b_x$,$b_n$ | width of hob cutter at varying pitch line, respectively (Fig. 3) |
| $C_1$ | center distance of hob cutter and RA worm gear (Fig. 5) |
| $d_x$ | distance measured from the middle of hob cutter tooth height to the varying pitch line (Figs. 2 and 3(b)) |
| $h$ | straight-lined edge height of hob cutter cutting blade (Fig. 3(b)) |
| $h_t$ | whole cutting blade height of hob cutter (Fig. 3(b)) |
| $\mathbf{L}_{ij}$ | coordinate transformation matrix transforming from coordinate system $S_j$ to $S_i$ (Eqs. (26), (27), (29), and (31)) |
| $l_1$ | surface parameter of hob cutter (Fig. 3(b)) |
| $\mathbf{M}_{ij}$ | homogeneous coordinate transformation matrix transforming from coordinate system $S_j$ to $S_i$ (Eqs. (8), (9), (18), and (19)) |
| $m_n$ | normal modulus (Fig. 2) |
| $m_x$ | axial modulus (Figs. 2 and 7), and $m_x = m_n/\cos\lambda_1$ |
| $m_{21}$ | angular velocity ratio of hob cutter to RA worm gear (Eqs. (28), (33) and (34)) |
| $N_1$,$N_1^{(c)}$ | normal vectors of hob cutter tooth surface (Eqs. (12) and (15)) |
| $N_{x1}$, $N_{y1}$, $N_{z1}$ | components of the normal vector expressed in coordinate system $S_1$ (Eqs. (34)) |
| $p_1$ | lead-per-radian revolution of hob cutter blade surface (Fig. 4) |
| $\mathbf{R}_1$, $\mathbf{R}_2$ | position vectors of hob cutter and RA worm gear, respectively |
| $r_o$, $r_1$, $r_f$ | outside radius, pitch radius and root radius of hob cutter, respectively (Fig. 3(c)) |
| $r_2$ | pitch radius of RA worm gear |
| $r_c$ | circular tip radius of hob cutter (Fig. 3(b)) |
| $r_t$ | design parameter of hob cutter (Fig. 3) |
| $S_i$, $S_j$ | reference and rotational coordinate systems ($i = f, g, p$ and $j = c$, 1, 2, 3 ) |
| $T_1$, $T_2$ | number of teeth of hob cutter and RA worm gear, respectively |
| $t_c$, $t_t$ | transverse chordal thicknesses at pitch circle and throat circle of RA worm gear, respectively (Fig. 11) |
| $\mathbf{V}_{12}^{(1)}$ | relative velocity vector of hob cutter and RA worm gear expressed in coordinate system $S_1$ (Eqs. (22) and (33)) |
| $\mathbf{V}_i^{(1)}$ | velocity vectors of hob cutter and RA worm gear ($i = 1, 2$) expressed in coordinate system $S_1$ (Eqs. (22)) |
| $\alpha_1$ | pressure angle of hob cutter (Fig. 3(b)) |
| $\gamma_1$ | cross angle of hob cutter in generating RA worm gear (Fig. 5) |
| $\theta_1$ | rotation angle of hob cutter in screw surface generation (Fig. 4) |
| $\lambda_1$ | lead angle of hob cutter (Fig. 4) |
| $\phi_1$, $\phi_2$ | rotational angles of hob cutter and RA worm gear, respectively (Fig. 5) |
| $\omega_1$, $\omega_2$ | angular velocities of hob cutter and RA worm gear, respectively (Eqs. (24), (25), (28) and (33)) |
| $\boldsymbol{\omega}_i^{(j)}$ | angular velocity vectors, expressed in coordinate system $S_j$ ($j = 1, p$) of hob cutter and RA worm gear ($i = 1, g$) (Eqs. (23)–(26) and (28)) |

Buckingham [1] proposed how to design RA worm gears. Yang [5] proposed an interactive computer graphics program to apply to an optimum RA gear design. Siegal and Mabie [6] developed a method to maximize the ratio of recess action to approach action by determining the individual hob offsets for a pair of spur gears designed to operate at nonstandard center distance. Meng and Chen [7] investigated theoretically and experimentally the scuffing resistance of full RA gears, in comparison with semi RA and standard ones. It appeared that full RA gears might prefer the pitting resistance and plastic-flow state to scuffing resistance in some extent than those of the others. Wildhaber [8] used the surface curvatures to obtain an approximate tooth contact for some worm gears generated by oversize hob cutters. Winter and Wilkesmann [9], and Bosch [10] proposed different methods to obtain more precise worm gear drive surfaces. Fang and Tsay [11] developed the mathematical model of conventional worm gear drives.

Up to now, only few researches have been investigated on the RA worm gears. However, mathematical model, computer simulation, tooth contact analysis and stress analysis of RA worm gears have not been studied yet. The aim of this paper is to develop the mathematical model of the RA worm gears with double-depth teeth. According to the generation mechanism of RA worm gear drives and the theory of gearing [12], the mathematical model of the RA worm gears can be derived. Three types of worm gear teeth, semi RA, full RA and standard proportional tooth, are concerned in this study. Based on the developed mathematical model, the computer graphs of semi RA, full RA and the standard proportional tooth worm gears can be plotted. Tooth surface variations of the RA worm gear teeth, due to the varying pitch line, pressure angle and tooth height of the hob cutter, are also investigated. The results of this study can be applied to further investigations on tooth contact analysis, kinematic errors, contact paths and contact patterns of the semi RA, full RA and standard proportional tooth worm gear drives.

## 2. Approach action and recess action of meshings for the semi RA, full RA and standard proportional tooth worm gear drives

Fig. 1 shows three types of worm gear drive meshing, semi RA, full RA and standard proportional tooth worm gear drives, with double-depth teeth at the same standard center distance. Fig. 1(a) shows the worm gear drive with standard proportional tooth

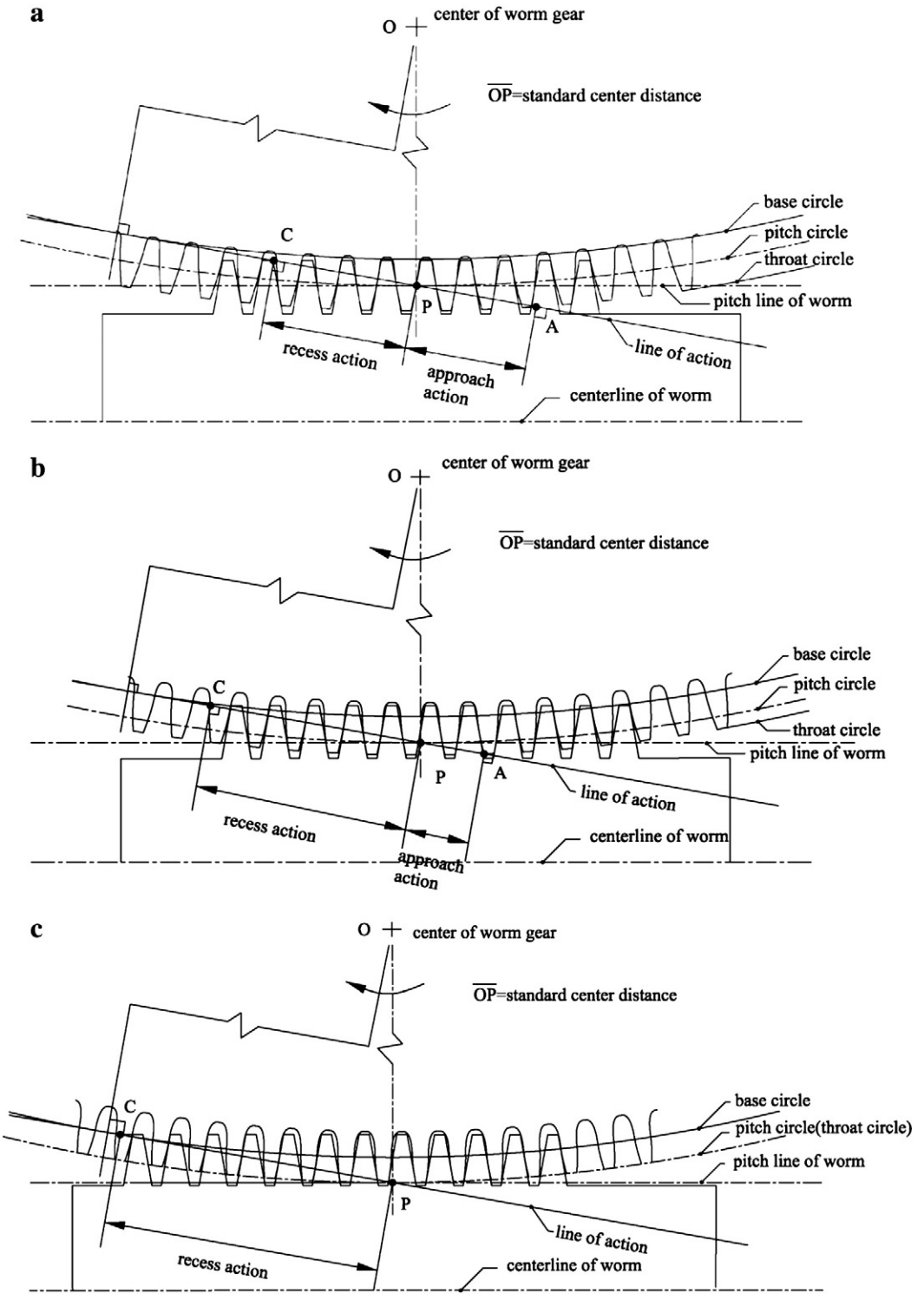


**Fig. 1.** Schematic figures of approach action and recess action for (a) standard proportional tooth (b) semi RA and (c) full RA worm gear drives.

meshing system. As contact progresses from point A (starting point of tooth engagement) to point P (pitch point), there is an approach action, while recess action occurs from point P to point C (final point of tooth engagement). It is noted that two parts of line of action for approach action and recess action are of equal contributions. In the gear meshing period, the approach action is a sliding-in process, and is the main resource of forming the friction than recess action. It is a detrimental scraping action, which tends to wear out the surface of gears. The friction is high, and it causes scuffing and noise. Nevertheless, the recess action is a

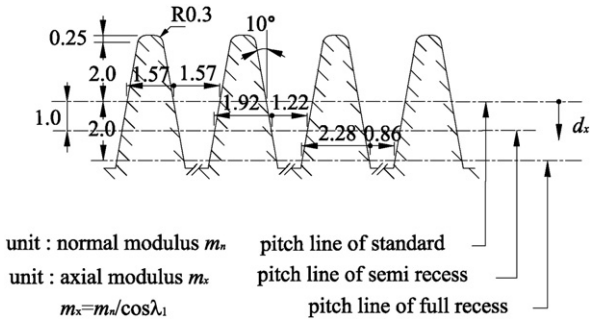


**Fig. 2.** Normal section of hob cutter with double-depth teeth, low pressure angle and varying pitch lines.

sliding-out meshing process to help keeping the rotation of worm gear drives in their respective directions, and friction is lower. Nature of the recess action is beneficial, tending to cold work the surfaces, smooth out the rough spots, and work-harden the contact surface in the gear meshing process. This in turn increases the surface endurance limits of the material and the load capacity [1].

The RA gear can eliminate the amount of friction by reducing the approach action, or increasing the recess action. Fig. 1(c) is the full RA worm gear meshing system obtained by having the pitch line of the worm tangent to the throat circle of the worm gear. In this case, the pitch circle and throat circle of the full RA worm gear are identical. The worm is made larger and the worm gear is smaller, so that the lead of worm is equal to the circular pitch of the worm gear at pitch circle or throat circle. This results in the existence of only the recess action in the process of worm gear drive mating. As shown in Fig. 1(b) and (c), both semi RA and full RA worm gear drives have a change in the contact conditions between engaging teeth. Most or all of the contact occurs during the recess action of line of contact. Thus, they can eliminate the detrimental effects of the approach action. This results in lower meshing torques and higher operating efficiency. It is frequently possible that the RA worm gear drive runs in a dry film lubrication in some cases whereas a conventional standard worm gear drive system would require a wet lubricant.

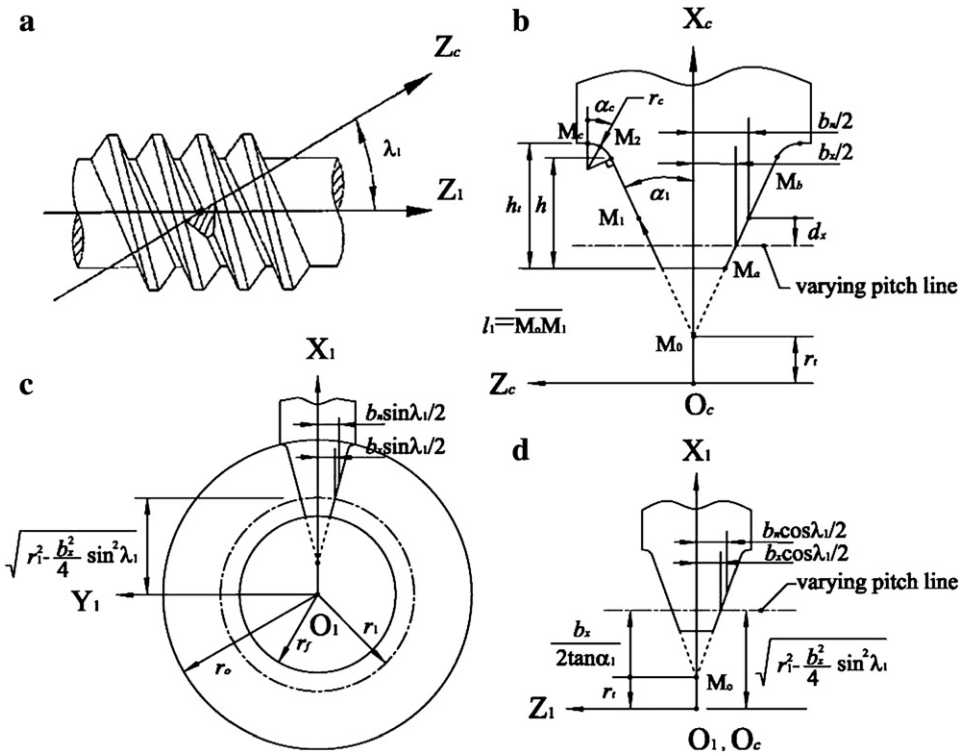


**Fig. 3.** ZN worm-type hob cutter with varying pitch lines represented by parameter $d_x$.

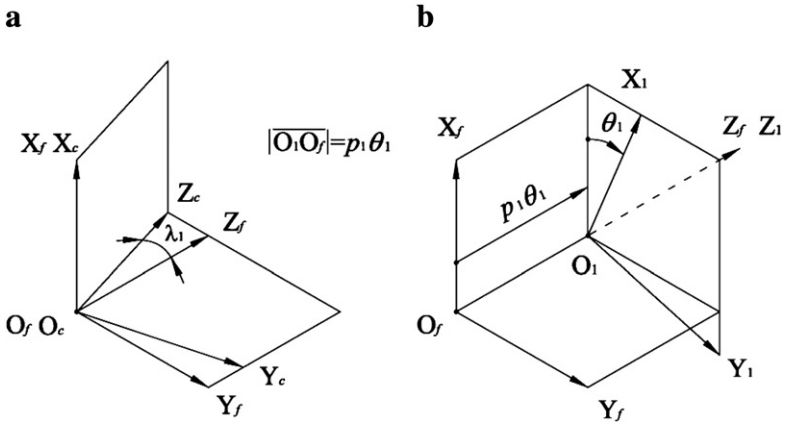


**Fig. 4.** Coordinate systems for (a) hob cutter setting with an inclined lead angle and (b) screw surface generation of ZN worm-type hob cutter.

Another advantage of RA worm gears is to balance strength. In general, for the standard proportional tooth worm gear drive, the tooth thicknesses of worm and worm gear at pitch circle are the same. However, a long-addendum design together with a proportional increase in tooth thickness at the pitch line of the worm [1,13] makes the tooth thickness of the worm gear at pitch circle is smaller for the RA worm gear drive, it makes the worm tooth stronger and the worm gear tooth weaker.

## 3. RA worm gears with double-depth teeth generated by different recess of hob cutters

RA worm gears can be manufactured with a standard hob cutter and hobbing machine, but consideration on varying pitch line of hob cutter with respect to the generated RA worm gears is needed. In this study, let's design the hob cutter different from the conventional one. Fig. 2 shows the normal section of hob cutter that its tooth form is a straight-lined edge shape based on the ZN worm-type of ISO classification. To design RA worm gear drives with double-depth teeth, the pressure angle of hob cutter is reduced from the normally used 20° and 22.5° to a minimum of 10° [2]. This should pay more attention on the checking of the teeth of hob cutter and generated RA worm gear should not be pointed. The pitch lines of the hob cutter in generating semi RA and full RA worm gears become $d_x = 1.0$ and 2.0 of normal modulus, $m_n$ (i.e. axial modulus $m_x = m_n/\cos\lambda_1$), below the middle of cutting tooth height, respectively, as shown in Fig. 2 where $d_x$ is the distance measured from the middle of cutting blade height to the varying pitch line (also refer to Fig. 3(b) and (d)). Thus, tooth thicknesses of the generated semi RA and full RA worm gears at their normal pitch circles become 1.22 and $0.86m_n$, and their normal throat radii are $(T_2+2)m_n/2$mm and $T_2m_n/2$mm, individually. Symbol $T_2$ denotes the tooth number of the generated RA worm gear. The above design gives different proportional changes of addendum and dedendum of hob cutter in generating semi RA and full RA worm gears. Especially, for a full RA worm gear, the pitch circle and throat circle are identical. Besides, the standard proportional tooth worm gear is a special case of the RA type worm gear when $d_x$ equals 0, no doubt, the pitch line of the hob cutter is at the middle of cutting tooth height. This gives that tooth thickness of the generated worm gear at its normal pitch circle is $1.57m_n$, and normal throat radius is $(T_2+4)m_n/2$mm.

## 4. Equation of the ZN worm -type hob cutter

The ZN worm-type hob cutter with normal profile of straight-lined edge shape is chosen to generate the RA worm gear in this study. A right-handed ZN worm-type hob cutter, as shown in Fig. 3, is chosen to generate RA worm gears in this study. The surfaces of ZN worm-type hob cutter can be cut by a blade. At first, the cutting blade is placed on the groove normal plane of the ZN worm-type hob cutter, as shown in Fig. 3(a). The blade, inclining with a lead angle $\lambda_1$ , is performed a screw motion with respect to the hob cutter axis.

According to Fig. 3(b), the normal section of the cutting blade consists of straight-lined edge and circular tip, which generate the tooth surface and fillet surface of the worm gear, respectively.

In Fig. 3(b), $l_1$ denotes a design parameter of the cutting blade straight-lined edge surface, starting from the intersection point $M_o$ of the two straight-lined edges to the end point $M_b$. And the moving point $M_1$, represents any point on the cutting blade straight-lined edge surface, moving from the initial point $M_a$ to the end point $M_b$. $\overline{M_oM_a}$ denotes the shortest distance of the cutting blade straight-lined edge surface, i.e. $l_{1(\min)}$, while $\overline{M_oM_b}$ indicates the longest distance of the cutting blade straight-lined edge surface, i.e. $l_{1(\max)}$.$\alpha_1$ denotes the pressure angle formed by the straight-lined edge and the $X_c$-axis, as shown in Fig. 3(b). The cutting blade width $b_x$ equals the normal groove width of the hob cutter, varying with the pitch line of the hob cutter in generating RA worm gears, as explained in Section 3. In Fig. 3(c), symbols $r_o$, $r_1$ and $r_f$ represent the outside radius, pitch radius and root radius of the ZN worm-type hob cutter, respectively.

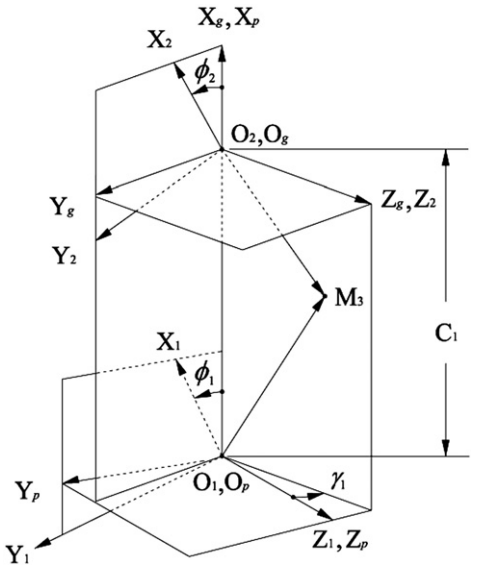


**Fig. 5.** Coordinate systems between ZN worm-type hob cutter and RA worm gear.

Therefore, the generating line of cutting blade can be represented in coordinate system $S_c(X_c, Y_c, Z_c)$ that fixed to the blade normal plane, as shown in Fig. 3(b), as follows:

$$R_c = \begin{bmatrix} r_t + l_1 \cos\alpha_1 \\ 0 \\ \pm l_1 \sin\alpha_1 \\ 1 \end{bmatrix}, \tag{1}$$

where the upper sign of "±" sign denotes the left-side of cutting blade while the lower sign denotes the right-side of cutting blade. $r_t$ is the distance measured from the rotation center of ZN worm-type hob cutter $O_1$ or $O_c$ to point $M_o$, as shown in Fig. 3(b) and (d). Therefore, $r_t$, $b_x$, $l_{1(\min)}$, $l_{1(\max)}$ and $h$ can be expressed as follows:

$$r_t = \sqrt{r_1^2 - \left(\frac{b_x}{2}\sin\lambda_1\right)^2} - \frac{b_x}{2\tan\alpha_1}, \tag{2}$$

$$b_x = b_n - 2d_x\tan\alpha_1, \tag{3}$$

$$l_{1(\min)} = \frac{1}{2\cos\alpha_1}\left(\frac{b_n}{\tan\alpha_1} - h\right), \tag{4}$$

$$l_{1(\max)} = \frac{1}{2\cos\alpha_1}\left(\frac{b_n}{\tan\alpha_1} + h\right). \tag{5}$$

**Table 1**
Design parameters of hob cutter and worm gear.

| Design parameter | Hob cutter | RA worm gear |
|---|---|---|
| Normal modulus | 1.97 mm/teeth | 1.97 mm/teeth |
| Axial modulus | 2 mm/teeth | 2 mm/teeth |
| Number of teeth | 3 | 337 |
| Lead angle | 10° | 80° |
| Pressure angle | 10° | 10° |
| Whole tooth height | 8.5 mm | 8.5 mm |
| Pitch radius | 17.02 mm | 337.00 mm |
| Circular tip radius | 0.6 mm | – |
| Throat height | – | 2 mm |
| Face width | – | 24 mm |
| Cutting center distance | 354.02 mm | |
| Cutting cross angle | 90° | |

and

$$h = h_t - r_c(1-\sin\alpha_1), \tag{6}$$

where $b_n$ is the blade width at the middle of cutting blade height, and $b_n = \pi m_n/2$, $h$ and $h_t$ denote straight-lined edge height and whole height of the cutting blade, respectively, and $r_c$ represents the cutting blade tip radius, and $d_x$ is the distance measured from the middle of cutting blade height to the varying pitch line of the hob cutter. A special case is $d_x = 0$ mm for generating the standard proportional tooth worm gear.

Similarly, the circular tip of cutting blade can also be expressed in coordinate system $S_c$ as follows:

$$R_c^{(c)} = \begin{bmatrix} r_t + \dfrac{b_n}{2\tan\alpha_1} + \dfrac{h}{2} + r_c(\cos\alpha_c - \sin\alpha_1) \\ 0 \\ \pm\left[\dfrac{b_n}{2} + \dfrac{h\tan\alpha_1}{2} + r_c(\cos\alpha_1 - \sin\alpha_c)\right] \\ 1 \end{bmatrix}, \tag{7}$$

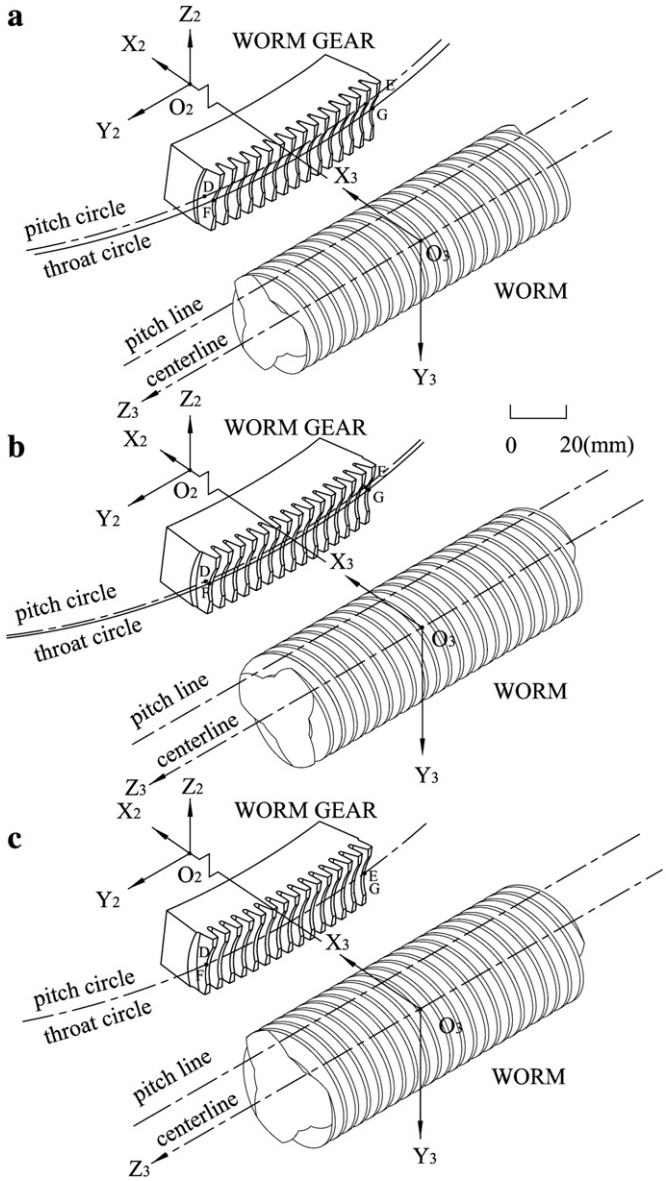


**Fig. 6.** Partial worm gear drive tooth profiles of (a) standard proportional teeth (b) semi RA teeth and (c) full RA teeth.

where $0 \le \alpha_c \le 90^\circ - \alpha_1$, and $\alpha_c$ denotes the angular design parameter of hob cutter circular tip. The moving point $M_2$ represents any point on the cutting blade circular tip surface moving from the initial point $M_c$ to the end point $M_b$.

Fig. 4 shows the relationship among the coordinate systems $S_c(X_c, Y_c, Z_c)$, $S_1(X_1, Y_1, Z_1)$ and $S_f(X_f, Y_f, Z_f)$, where $S_c$ is the blade coordinate system, coordinate system $S_1$ is rigidly connected to the hob cutter tooth surface, and $S_f$ is the reference coordinate system. The inclined angle $\lambda_1$, formed by axes $Z_c$ and $Z_f$, is the lead angle of hob cutter. The tooth surface equation of the ZN worm-type hob cutter can be obtained by considering the blade coordinate system (i.e.$S_c$) performs a screw motion with respect to the fixed coordinate system $S_f$. This can be achieved by applying the following homogeneous coordinate transformation matrix equation:

$$R_1 = M_{1f} M_{fc} R_c = M_{1c} R_c, \tag{8}$$

where

$$M_{1c} = \begin{bmatrix} \cos\theta_1 & \cos\lambda_1 \sin\theta_1 & -\sin\lambda_1 \sin\theta_1 & 0 \\ -\sin\theta_1 & \cos\lambda_1 \cos\theta_1 & -\sin\lambda_1 \cos\theta_1 & 0 \\ 0 & \sin\lambda_1 & \cos\lambda_1 & -p_1\theta_1 \\ 0 & 0 & 0 & 1 \end{bmatrix}, \tag{9}$$

and $p_1$ indicates the lead-per-radian revolution of the hob cutter surface, and $\theta_1$ denotes the rotational angle of the hob cutter in relevant screw motion. Substituting Eqs. (1) and (9) into Eq. (8), the straight-line edge surface equation of ZN worm-type hob cutter $\mathbf{R}_1$ can be represented in coordinate system $S_1$ as follows:

$$R_1 = \begin{bmatrix} (r_t + l_1 \cos\alpha_1)\cos\theta_1 \mp l_1 \sin\lambda_1 \sin\alpha_1 \sin\theta_1 \\ -(r_t + l_1 \cos\alpha_1)\sin\theta_1 \mp l_1 \sin\lambda_1 \sin\alpha_1 \cos\theta_1 \\ \pm l_1 \cos\lambda_1 \sin\alpha_1 - p_1\theta_1 \\ 1 \end{bmatrix}. \tag{10}$$

Similarly, substituting Eqs. (7) and (9) into Eq. (8), the circular tip surface equation of the ZN worm-type hob cutter $\mathbf{R}_1^{(c)}$ can also be obtained as follows:

$$R_1^{(c)} = \begin{bmatrix} \cos\theta_1 \left[ r_t + \dfrac{b_n}{2\tan\alpha_1} + \dfrac{h}{2} + r_c(\cos\alpha_c - \sin\alpha_1) \right] \mp \\ \sin\lambda_1 \sin\theta_1 \left[ \dfrac{b_n}{2} + \dfrac{h\tan\alpha_1}{2} + r_c(\cos\alpha_1 - \sin\alpha_c) \right] \\ -\sin\theta_1 \left[ r_t + \dfrac{b_n}{2\tan\alpha_1} + \dfrac{h}{2} + r_c(\cos\alpha_c - \sin\alpha_1) \right] \mp \\ \sin\lambda_1 \cos\theta_1 \left[ \dfrac{b_n}{2} + \dfrac{h\tan\alpha_1}{2} + r_c(\cos\alpha_1 - \sin\alpha_c) \right] \\ \cos\lambda_1 \left[ \dfrac{b_n}{2} + \dfrac{h\tan\alpha_1}{2} + r_c(\cos\alpha_1 - \sin\alpha_c) \right] - p_1\theta_1 1 \end{bmatrix}. \tag{11}$$

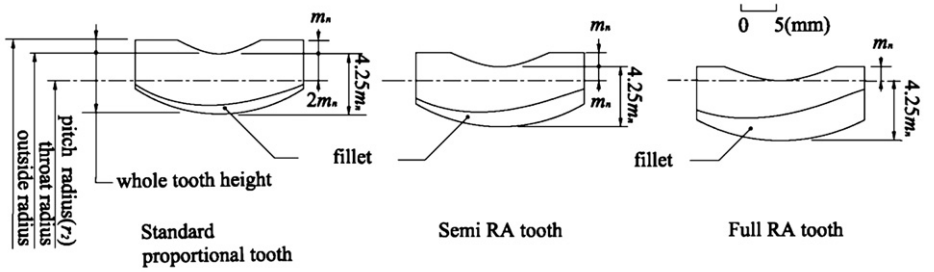


| | Standard proportional tooth | Semi RA tooth | Full RA tooth |
|---|---|---|---|
| Pitch radius ($r_2$) | 337.00mm | 337.00mm | 337.00mm |
| Throat height | $m_n$ | $m_n$ | $m_n$ |
| Throat radius | $r_2 + 2m_n$ | $r_2 + m_n$ | $r_2$ |
| Outside radius | $r_2 + 3m_n$ | $r_2 + 2m_n$ | $r_2 + m_n$ |

Note: $m_x = m_n / \cos\lambda_1$

**Fig. 7.** Comparison of axial cross sections of worm gear teeth.

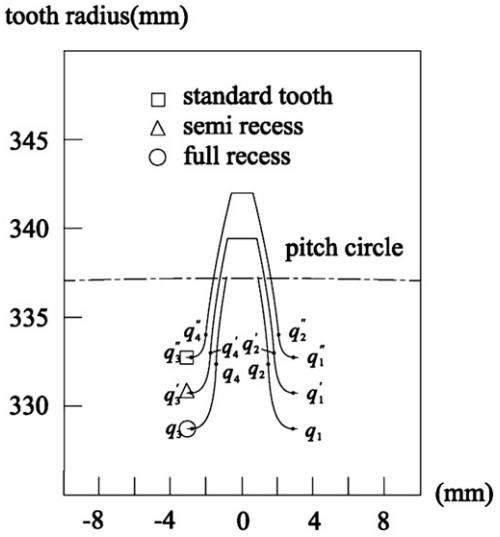


**Fig. 8.** Comparison of tooth profiles for semi RA, full RA and standard proportional tooth worm gears at cross-section of $Z_2 = 0$ mm.

## 5. Normal equation of the ZN worm-type hob cutter

The normal vector of the hob cutter straight-lined edge surface, represented in the coordinate system$S_1$, can be obtained by:

$$N_1 = \frac{\partial R_1}{\partial l_1} \times \frac{\partial R_1}{\partial \theta_1}, \tag{12}$$

where

$$\frac{\partial R_1}{\partial l_1} = \begin{bmatrix} \cos\alpha_1 \cos\theta_1 \mp \sin\alpha_1 \sin\lambda_1 \sin\theta_1 \\ -\cos\alpha_1 \sin\theta_1 \mp \sin\alpha_1 \sin\lambda_1 \cos\theta_1 \\ \pm \sin\alpha_1 \cos\lambda 1 \end{bmatrix}, \tag{13}$$

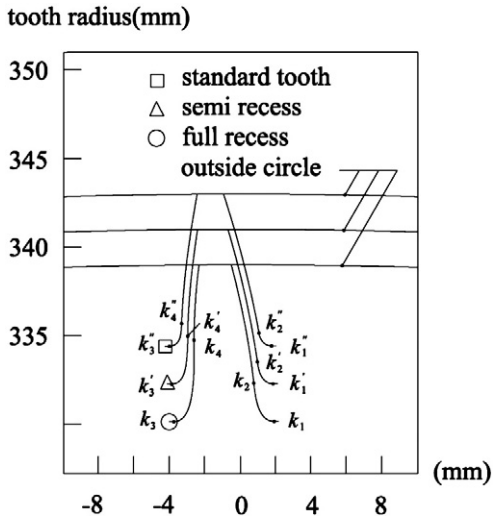


**Fig. 9.** Comparison of tooth profiles for semi RA, full RA and standard proportional tooth worm gears at cross-section of $Z_2 = 8$ mm.

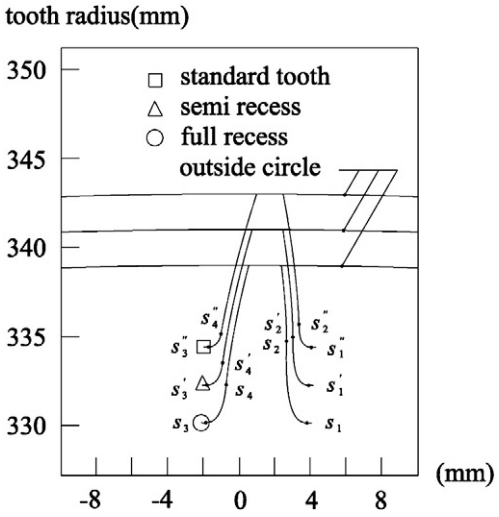


**Fig. 10.** Comparison of tooth profiles for semi RA, full RA and standard proportional tooth worm gears at cross-section of $Z_2 = -8$ mm.

and

$$\frac{\partial R_1}{\partial \theta_1} = \begin{bmatrix} -(r_t + l_1 \cos\alpha_1)\sin\theta_1 \mp l_1 \sin\lambda_1 \sin\alpha_1 \cos\theta_1 \\ -(r_t + l_1 \cos\alpha_1)\cos\theta_1 \pm l_1 \sin\lambda_1 \sin\alpha_1 \sin\theta_1 \\ -p_1 \end{bmatrix}. \tag{14}$$

Similarly, the normal vector of the hob cutter circular tip surface, also represented in the coordinate system $S_1$, can be obtained by:

$$N_1^{(c)} = \frac{\partial R_1^{(c)}}{\partial \alpha_c} \times \frac{\partial R_1^{(c)}}{\partial \theta_1}, \tag{15}$$

where

$$\frac{\partial R_1^{(c)}}{\partial \alpha_c} = \begin{bmatrix} r_c(-\sin\alpha_c \cos\theta_1 \pm \sin\lambda_1 \cos\alpha_c \sin\theta_1) \\ r_c(\sin\alpha_c \sin\theta_1 \pm \sin\lambda_1 \cos\alpha_c \cos\theta_1) \\ -r_c \cos\lambda_1 \cos\alpha_c \end{bmatrix}, \tag{16}$$

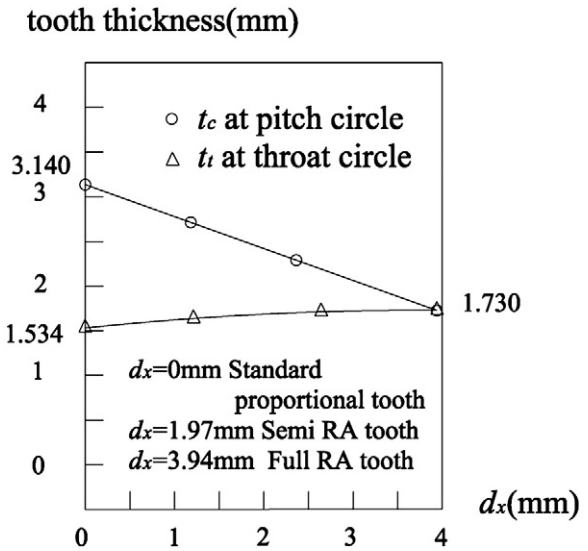


**Fig. 11.** Transverse chordal thickness of RA worm gears with varying pitch lines at cross-section $Z_2 = 0$ mm.

and

$$\frac{\partial R_1^{(c)}}{\partial \theta_1} = \begin{bmatrix} -\sin\theta_1\left[r_t + \dfrac{b_n}{2\tan\alpha_1} + \dfrac{h}{2} + r_c(\cos\alpha_c - \sin\alpha_1)\right] \mp \\ \sin\lambda_1\cos\theta_1\left[\dfrac{b_n}{2} + \dfrac{h\tan\alpha_1}{2} + r_c(\cos\alpha_1 - \sin\alpha_c)\right] \\ -\cos\theta_1\left[r_t + \dfrac{b_n}{2\tan\alpha_1} + \dfrac{h}{2} + r_c(\cos\alpha_c - \sin\alpha_1)\right] \pm \\ \sin\lambda_1\sin\theta_1\left[\dfrac{b_n}{2} + \dfrac{h\tan\alpha_1}{2} + r_c(\cos\alpha_1 - \sin\alpha_c)\right] \\ -p_1 \end{bmatrix}. \tag{17}$$

## 6. Mathematical equation of the generated RA worm gears

Fig. 5 shows the schematic generating mechanism of hob cutter and RA worm gear. Coordinate systems $S_p(X_p, Y_p, Z_p)$and $S_g(X_g, Y_g, Z_g)$ are reference coordinate systems for the hob cutter and generated RA worm gear, respectively. Coordinate system $S_1(X_1, Y_1, Z_1)$ of the hob cutter rotates through an angle $\phi_1$ counterclockwise with respect to the reference coordinate system $S_p$. Similarly, coordinate system $S_2(X_2, Y_2, Z_2)$ of the generated RA worm gear rotates through an angle $\phi_2$ counterclockwise with respect to the reference coordinate system $S_g$. Reference coordinate systems $S_p$ and $S_g$ are formed a cutting cross angle $\gamma_1$ of the hob cutter and generated RA worm gear. $\overline{O_1O_2} = C_1$ is the center distance of the hob cutter and generated RA worm gear, i.e.$C_1 = r_1 + r_2$, where $r_1$ and $r_2$ are the pitch radii of hob cutter and generated RA worm gear, respectively.

The locus equation of hob cutter surface can be obtained by applying the following homogeneous coordinate transformation matrix equation:

$$R_2 = M_{2g}M_{gp}M_{p1}R_1 = M_{21}R_1, \tag{18}$$

where

$$M_{21} = \begin{bmatrix} a_{11} & a_{12} & \sin\gamma_1\sin\phi_2 & -\cos\phi_2 C_1 \\ a_{21} & a_{22} & \sin\gamma_1\cos\phi_2 & \sin\phi_2 C_1 \\ -\sin\gamma_1\sin\phi_1 & -\sin\gamma_1\cos\phi_1 & \cos\gamma_1 & 0 \\ 0 & 0 & 0 & 1 \end{bmatrix}, \tag{19}$$

and

$$\begin{aligned} a_{11} &= +\cos\phi_1\cos\phi_2 + \cos\gamma_1\sin\phi_1\sin\phi_2, \\ a_{12} &= -\sin\phi_1\cos\phi_2 + \cos\gamma_1\cos\phi_1\sin\phi_2, \\ a_{21} &= -\cos\phi_1\sin\phi_2 + \cos\gamma_1\sin\phi_1\cos\phi_2, \\ a_{22} &= +\sin\phi_1\sin\phi_2 + \cos\gamma_1\cos\phi_1\cos\phi_2. \end{aligned} \tag{20}$$

By substituting Eqs. (10), (11) and (19) into Eq. (18), the hob cutter locus equations of straight-lined edge and circular tip, expressed in coordinate system $S_2$, are obtained as follows:

$$R_2 = \begin{bmatrix} a_{11}X_1 + a_{12}Y_1 + \sin\gamma_1\sin\phi_2 Z_1 - \cos\phi_2 C_1 \\ a_{21}X_1 + a_{22}Y_1 + \sin\gamma_1\cos\phi_2 Z_1 + \sin\phi_2 C_1 \\ -\sin\gamma_1\sin\phi_1 X_1 - \sin\gamma_1\cos\phi_1 Y_1 + \cos\gamma_1 Z_1 \\ 1 \end{bmatrix}, \tag{21}$$

where $\phi_2 = \frac{T_1}{T_2}\phi_1$, and $T_1$, $T_2$, $\phi_1$, and $\phi_2$ are tooth numbers and rotational angles of the hob cutter and generated RA worm gear, respectively.

## 7. Equation of meshing between the hob cutter and generated RA worm gears

In the worm gear generation process, the hob cutter and generated RA worm gear tooth surfaces are never embedded into each other, i.e. the relative velocity of the generated RA worm gear with respect to the hob cutter is perpendicular to their common normal vector $\mathbf{N}_1$ at any cutting instant. Therefore, the equation of meshing of the hob cutter and generated RA worm gear can be expressed as follows [12]:

$$N_1 \bullet V_{12}^{(1)} = N_1 \bullet \left(V_1^{(1)} - V_2^{(1)}\right) = 0, \tag{22}$$

where $\mathbf{V}_1^{(1)}$ and $\mathbf{V}_2^{(1)}$ denote the velocities of the hob cutter and generated RA worm gear, respectively, and superscript " (1) " indicates the velocities are represented in coordinate system $S_1$.

According to Fig. 5, the relative velocity of the generated RA worm gear with respect to the hob cutter represented in coordinate system $S_1$, can be obtained by:

$$V_{12}^{(1)} = \left(\omega_1^{(1)} - \omega_2^{(1)}\right) \times R_1 - \overline{O_1O_2}(1) \times \omega_2^{(1)}, \tag{23}$$

where $\boldsymbol{\omega}_1^{(1)}$ and $\boldsymbol{\omega}_2^{(1)}$ are the angular velocities of the hob cutter and the generated RA worm gear, respectively, and they can be expressed in their respectively coordinate systems $S_1$ and $S_g$ as follows:

$$\omega_1^{(1)} = [0 \quad 0 \quad 1]^T \omega_1, \tag{24}$$

and

$$\omega_2^{(g)} = [0 \quad 0 \quad 1]^T \omega_2. \tag{25}$$

Angular velocity $\boldsymbol{\omega}_2^{(g)}$can be also represented in coordinate system $S_1$, by applying the following coordinate transformation matrix equation:

$$\omega_2^{(1)} = L_{1p} L_{pg} \omega_2^{(g)} = L_{1g} \omega_2^{(g)}, \tag{26}$$

where

$$L_{1g} = \begin{bmatrix} \cos\phi_1 & \cos\gamma_1 \sin\phi_1 & -\sin\gamma_1 \sin\phi_1 \\ -\sin\phi_1 & \cos\gamma_1 \cos\phi_1 & -\sin\gamma_1 \cos\phi_1 \\ 0 & \sin\gamma_1 & \cos\gamma_1 \end{bmatrix}. \tag{27}$$

Substituting Eqs. (25) and (27) into Eq. (26), the angular velocity of the generated RA worm gear, represented in coordinate system $S_1$, can be obtained by:

$$\omega_2^{(1)} = \omega_1 \begin{bmatrix} -m_{21} \sin\gamma_1 \sin\phi_1 \\ -m_{21} \sin\gamma_1 \cos\phi_1 \\ m_{21} \cos\gamma_1 \end{bmatrix}, \tag{28}$$

where $m_{21} = \phi_2/\phi_1$ is the angular velocity ratio of generated RA worm gear to hob cutter.

Similarly, according to Fig. 5, vector $\overline{O_1O_2}$ can be obtained and expressed in coordinate system $S_1$ by

$$\overline{O_1O_2}^{(1)} = L_{1p} \overline{O_1O_2}^{(p)}, \tag{29}$$

where

$$\overline{O_1O_2}^{(p)} = [C_1 \quad 0 \quad 0]^T, \tag{30}$$

and

$$L_{1p} = \begin{bmatrix} \cos\phi_1 & \sin\phi_1 & 0 \\ -\sin\phi_1 & \cos\phi_1 & 0 \\ 0 & 0 & 1 \end{bmatrix}. \tag{31}$$

Substituting Eqs. (30) and (31) into Eq. (29), vector $\overline{O_1O_2}$ is represented in coordinate system $S_1$ as follows:

$$\overline{O_1O_2}^{(1)} = \begin{bmatrix} \cos\phi_1 C_1 \\ -\sin\phi_1 C_1 \\ 0 \end{bmatrix}. \tag{32}$$

Again, substituting Eqs. (10), (11), (24), (28), and (32) into Eq. (23) yields:

$$V_{12}^{(1)} = \omega_1 \begin{bmatrix} (m_{21}\cos\gamma_1 - 1)Y_1 + m_{21}(\sin\gamma_1 \cos\phi_1 Z_1 + \cos\gamma_1 \sin\phi_1 C_1) \\ -(m_{21}\cos\gamma_1 - 1)X_1 + m_{21}(-\sin\gamma_1 \sin\phi_1 Z_1 + \cos\gamma_1 \cos\phi_1 C_1) \\ m_{21}\sin\gamma_1(-\cos\phi_1 X_1 + \sin\phi_1 Y_1 + C_1) \end{bmatrix}. \tag{33}$$

Eq. (33) expresses the relative velocity of the hob cutter and generated RA worm gear at their common cutting point $M_2$ at every cutting instant. According to theory of gearing, the common surface normal $\mathbf{N}_1$ is perpendicular to relative velocity $\mathbf{V}_{12}^{(1)}$. Therefore, substituting Eqs. (12), (15) and (33) into Eq. (22) obtains:

$$\begin{aligned} f(l_1,\theta_1,\phi_1(\phi_2)) = {} & [(m_{21}\cos\gamma_1 - 1)Y_1 + m_{21}(\sin\gamma_1\cos\phi_1 Z_1 + \cos\gamma_1\sin\phi_1 C_1)]N_{x1} + \\ & [-(m_{21}\cos\gamma_1 - 1)X_1 + m_{21}(-\sin\gamma_1\sin\phi_1 Z_1 + \cos\gamma_1\cos\phi_1 C_1)]N_{y1} + \\ & [m_{21}\sin\gamma_1(-\cos\phi_1 X_1 + \sin\phi_1 Y_1 + C_1)]N_{z1} = 0, \end{aligned} \tag{34}$$

where $N_{x1}$, $N_{y1}$ and $N_{z1}$ are components of the normal vector of hob cutter.

Eq. (34) is the so-called equation of meshing of the hob cutter and generated RA worm gear. This equation keeps them in tangency at every instant during the cutting process. Therefore, the working tooth and fillet surface equations of the generated RA worm gear can be obtained by considering the hob cutter locus equations of straight-lined edge and circular tip as well as the equations of meshing, i.e. Eqs. (21) and (34), simultaneously.

## 8. Computer graphs of the generated RA worm gears with double-depth teeth

The tooth surface equation of the generated RA worm gear proposed herein can be verified by plotting the worm gear profile with computer graphics. Since the tooth surface equation is non-linear, therefore, solving by numerical analysis method is needed.

Table 1 lists some design parameters of the hob cutter and generated RA worm gear. Based on the developed mathematical model of the worm gear tooth surface, three-dimensional tooth profiles of semi RA, full RA and standard proportional tooth worm gears are plotted in Fig. 6. A series of worm gears, partial (15/337) teeth are plotted, are of the same pitch circle and throat height, but with different throat circle and outside circle. Points D and E indicate the penetration points of pitch circle with partial (15/337) teeth, while points F and G are the intersection points of the throat circle with generated worm gear. For a full RA worm gear, pitch circle and throat circle pass through the throat of the worm gear, as shown in Fig. 6(c). In the other words, pitch circle and throat circle are identical. But for the standard proportional tooth worm gear (i.e. special case of RA worm gear with $d_x = 0$), pitch circle passes through the middle of the tooth height, as shown in Fig. 6(a).

## 9. Tooth profile comparisons of the generated RA worm gears with double-depth teeth

The worm gear design parameters are chosen the same as those listed in Table 1. A series of worm gears, semi RA, full RA and the standard proportional tooth, are generated by using varying pitch lines (refer to Figs. 2 and 3), $d_x = 1.97$ mm, 3.94 mm and 0 mm, respectively. Axial cross sections of this series of worm gear teeth are shown in Fig. 7. Figs. 8, 9 and 10 show the tooth profiles of the generated RA worm gears with double-depth teeth at cross sections of $Z_2 = 0$ mm, $Z_2 = 8$ mm, and $Z_2 = -8$ mm (refer to Fig. 6), respectively.

Fig. 8 shows the tooth profiles of a series of worm gears at cross section of $Z_2 = 0$ mm. It is noted that for the full RA worm gear, its pitch circle and throat circle become identical (also refer to Figs. 6(c) and 7), only dedendum part of working height exists, and addendum part shrinks to zero, because of full recess design. Additionally, the fillet curves $q_1q_2$ and $q_3q_4$ of the full RA worm gear that generated by hob cutter are larger than those of two others, thus the working height is smaller. And, the standard proportional tooth worm gear is easier to become pointed teeth than the full RA type worm gear. Fig. 8 also shows that the transverse chordal tooth thickness of the full RA worm gear at pitch circle is the smallest.

Fig. 9 shows the tooth profiles having different outside circles at $Z_2 = 8$ mm. A series of worm gears have the constant lead angle across the whole face width. The standard proportional tooth worm gear has a thicker tooth, and the full RA type worm gear has a thinner tooth. Comparisons of Figs. 8 and 9 show that the thickness of standard proportional worm gear tooth profile is larger and its fillet curves $k_1''k_2''$ and $k_3''k_4''$ are smaller at the end of face width $Z_2 = 8$ mm. Comparisons of Figs. 8, 9 and 10 show that the RA worm gear fillet curves are the largest ones at $Z_2 = 0$ mm. A full RA worm gear tooth most likes a column across the whole face width.

Fig. 11 numerically shows the transverse chordal tooth thickness at pitch circle and throat circle, respectively, at the cross section $Z_2 = 0$ mm. It is found that the tooth thickness at pitch circle, $t_c = 3.140$ mm, is the largest for the standard proportional tooth worm gear than those for semi RA and full RA types. Reversely, the tooth thickness of the standard proportional tooth worm gear at throat circle, $t_t = 1.534$ mm, becomes the smallest. It is noted that the tooth thicknesses at pitch circle and throat circle are the same, $t_c = t_t = 1.730$ mm, for the full RA worm gear because its pitch circle and throat circle are identical.

## 10. Conclusion

The mathematical model of the generated RA worm gear with double-depth teeth is developed according to the gear generation mechanism and the theory of gearing. The tooth surface equation of the RA worm gear is also expressed in terms of design parameters of the ZN worm-type hob cutter. Computer graphs of semi RA, full RA and the standard proportional tooth worm gears are plotted. It is found that the pitch circle and throat circle of the full RA worm gear are identical. At cross-section of tooth cross-section of tooth width, i.e. $Z_2 = 0$ mm, the addendum part of the full RA worm gear shrinks to zero. Besides, the fillet curve of the full RA worm gear is longer

than those of semi RA and standard proportional worm gears. The transverse chordal tooth thickness of the full RA worm gear at pitch circle is smaller than those of the semi RA and standard proportional worm gears. The results of this study would be most helpful to the further studies of contact ellipse, contact path, kinematic errors (KEs), and stress analysis of the RA worm gear.

## References

[1] E.K. Buckingham, Here's How to Design Full and Semi-Recess Action Gears, Gear Design and Application, in: N.P. Chironis (Ed.), Product Engineering Magazine, 1971, pp. 136–143.
[2] E.K. Buckingham, 3 Are Familiar, 3 Little Known in this Guide to Worm Gear Types, Gear Design and Application, in: N.P. Chironis (Ed.), Product Engineering Magazine, 1971, pp. 69–78.
[3] W.P. Crosher, Design and Application of the Worm Gear, ASME Press, New York, 2002.
[4] J.E. Shigley, C.R. Mischke, Mechanical Engineering Design, 5th ed McGraw-Hill, NY, 1989.
[5] Y. Yang, Computer-aided design of recess-action gears, Computers in Engineering, Proceedings of the International Computers in Engineering Conference, 3, 1985, pp. 445–449.
[6] R.E. Siegal, H.H. Mabie, Determination of hob-offset values for nonstandard spur gears based on maximum ratio of recess to approach action, Appl. Mech. Conf., 3rd, Proc., Pap., Stillwater, 1973.
[7] H. Meng, Q. Chen, Research into the scuffing loading capacity of all-recess action gears, Proceedings of the Sixth World Congress on the Theory of Machines and Mechanisms, 1984, pp. 895–901.
[8] E. Wildhaber, A new look at worm gear hobbing, Proceedings of American Gear Manufactures Association Conference, Virginia, 1954.
[9] H. Winter, H. Wilkesmann, Calculation of cylindrical worm gear drives of different tooth profiles, J. Mech. Des., Trans. ASME 103 (1981) 73–82.
[10] M. Bosch, Economical Production of High Precision Gear Worms and Other Thread Shaped Profiles by Means of CNC-Controlled Worm and Thread Grinding Machines, Klingelnberg Publication, Germany, 1988, pp. 3–19.
[11] H.S. Fang, C.B. Tsay, Mathematical model and bearing contacts of the ZN-type worm gear sets cut by oversize hob cutters, Mech. Mach. Theor. 35 (12) (2000) 1689–1708.
[12] F.L. Litvin, A. Fuentes, Gear Geometry and Applied Theory, second ed. Cambridge University Press, 2004.
[13] D.W. Dudley, Handbook of Practical Gear Design, CRC Press, 1994.